Krishna R. Reddy,[1] *Surendra K. Saxena,*[2] *and Jeffry S. Budiman*[3]

Development of a True Triaxial Testing Apparatus

REFERENCE: Reddy, K. R., Saxena, S. K., and Budiman, J. S., **"Development of a True Triaxial Testing Apparatus,"** *Geotechnical Testing Journal*, GTJODJ, Vol. 15, No. 2, June 1992, pp. 89–105.

ABSTRACT: A stress-controlled, flexible boundary, true (or cubical) triaxial apparatus has been developed to investigate the behavior of cemented sand under various stress paths which are not achievable using conventional axisymmetric triaxial apparatus. The apparatus components, specimen preparation, and test procedure are described. Tests were performed on cemented sand along different stress paths which included hydrostatic compression, conventional triaxial compression, and along different directions on octahedral planes. The test results indicate that stress-strain and volumetric response of cemented sand depends on stress path.

KEY WORDS: laboratory tests, triaxial tests, stress, stress paths, sands, cementation, stress-strain behavior, shear strength, failure envelope

This paper describes the development of a true (or cubical) triaxial soil testing system which was utilized to investigate the constitutive behavior of cemented sand under different stress paths. Though the development of true triaxial devices dates back to the 1930s, it was only during the 1960s that such devices became popular, mostly due to their salient feature of enabling the generation of complete stress paths in the first octant of the stress space. Validation of constitutive models has become an important research effort in the past two decades, and the current soil modeling philosophy involves strong interaction and mutual feedback between analytical and experimental work. The experimental results obtained in true triaxial testing have become the benchmark to evaluate the capability of analytical models. The use of true triaxial devices has increased considerably since the 1970s when the introduction of personal computers and data acquisition systems at an affordable cost allowed the efficient recording and storage of data. Even though different types of true triaxial devices have been developed worldwide, all of them can be classified into three categories. They are: (1) rigid boundary type (Hambly 1969; Airey and Wood 1988), (2) flexible boundary type (Ko and Scott 1967; Sture and Desai 1979), and (3) mixed boundary type (Green 1971; Lade and Duncan 1973). The advantages and disadvantages of the three types of true triaxial devices have been discussed by Sture (1979) and Arthur (1988). The device described herein is a flexible boundary type with the cubical specimen seated between six rubber membranes. The original development of the device was presented by Ko and Scott (1967). The device permits the study of stress-strain response of soils under simple-to-complex stress paths under either drained or undrained conditions. Typical test results on cemented sand using the apparatus are presented and discussed in this paper.

[1]Geotechnical engineer, Patrick Engineering Inc., 346 Taft Avenue, Glen Ellyn, IL 60137.

[2]Deceased, formerly professor and chairman, Civil Engineering Department, Illinois Institute of Technology, Chicago, IL 60616.

[3]Visiting assistant professor, Civil Engineering Department, Illinois Institute of Technology, Chicago, IL 60616.

The Apparatus

The true triaxial device consists of the following components: a frame, six wall assemblies, a deformation measuring system, a stress application and control system, six membranes, a volume change monitoring system, a pore water pressure monitoring system, and a data acquisition system. A brief description of these components is provided below.

Frame. An isometric view and a photograph of the frame are shown in Figs. 1 and 2, respectively. The frame was machined from solid aluminum. The frame supports the wall assemblies and the specimen. A narrow recess was machined into each of the six faces of the frame to accommodate the membranes and to form pressure cavities. Connection bolts were provided on each face of the frame to fix the wall assemblies. Drainage and pore water pressure monitoring ports were machined diagonally through the frame.

Wall assemblies. Six wall assemblies also were machined from aluminum. Each wall assembly consists of a main cover plate which provides the wall seal for the interior pressure cavity and a pressure inlet connection. When membranes are attached, each assembly provides an effective seal against air leaking to the atmosphere. Four threaded holes were machined into each cover plate to receive stainless steel hollow tubes. The steel tubes were inserted in the holes and sealed with epoxy as shown in Fig. 3. The outer ends of the tubes were capped. The inside and outside diameters of each tube were machined to allow free movement of the core of a linear variable differential transformer (LVDT) within the tube and allow the LVDT coil to slide over the tube. Figure 4 shows a photograph of the wall assembly. The inside projection of the wall holds the membranes and seals the pressure cavity completely.

Deformation measuring system. The deformation of the specimen can be measured at four points on each of its six faces using 24 LVDTs. The core of each LVDT and its extension rod are thrust into contact with the specimen's membrane by a spring as shown in Fig. 5. The excitation and output of the LVDTs are controlled and recorded by a data acquisition system.

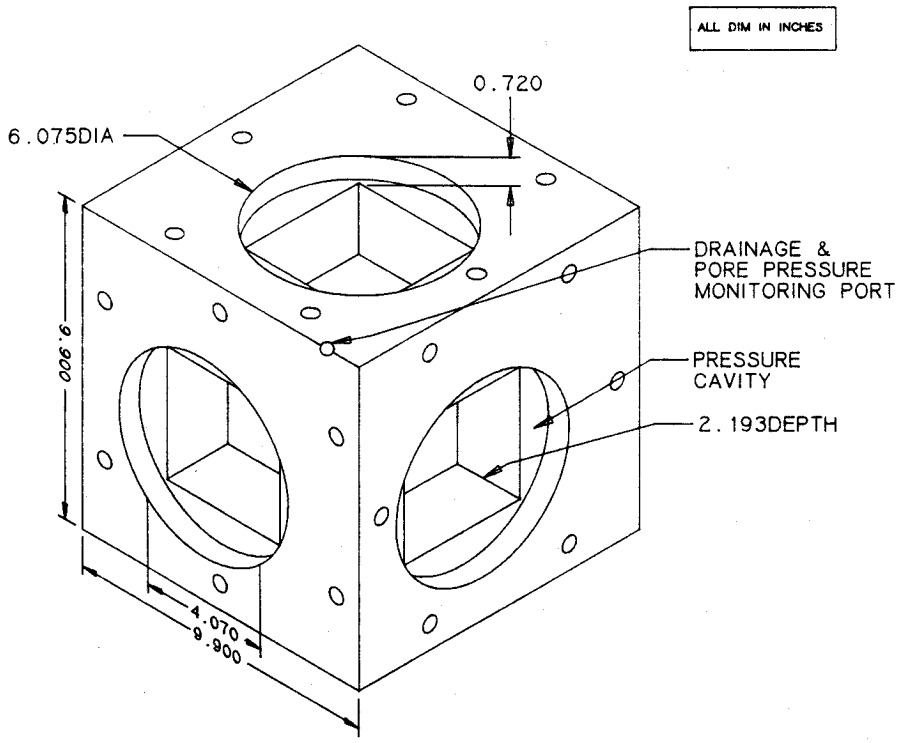

FIG. 1—*Isometric view of the frame.*

Stress application and control system. The stress control system developed in this study consisted of hand-operated precision pressure regulators, valves, and Bourdon tube pressure gages. A schematic of the stress control system is shown in Fig. 6. The system enables the operator to apply all three independent principal stresses to the specimen. Any stress path in the first octant can be achieved by simultaneous operation of the three pressure regulators. Three AP10, absolute pressure transducers manufactured by Validyne (Validyne Engineering, CA) were used to measure the pressures up to 200 psi (1378 kPa). The transducer output can be automatically recorded and stored by activating the data acquisition system.

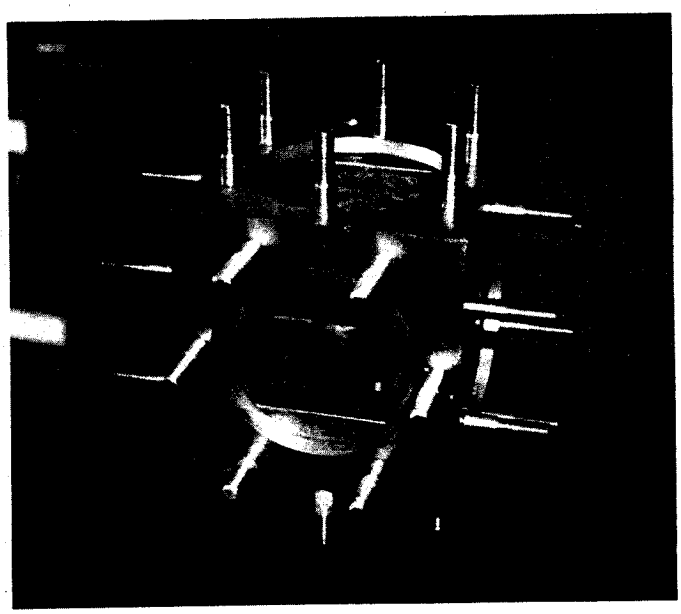

FIG. 2—*Photograph of the frame.*

Membranes. The membranes transmit the applied pressure uniformly to the soil specimen faces. The membranes were prepared in the laboratory using a silicone rubber possessing high tear strength and low stiffness. Dow Corning silicone rubber, a Silastic J-RTV type, was used in this study to make the membranes. An assembly consisting of top and bottom molds machined from aluminum was used to prepare membranes of design dimensions after allowing for shrinkage while curing. The silicone rubber and curing agent were mixed to a uniform consistency and deaired under vacuum for about 30 min. The mixture was then poured into the bottom mold. The mixture was again deaired under vacuum for about 30 min. Next, the top plate of the mold was carefully bolted in place and the mixture was allowed to cure for two days. The membrane was removed from the mold and stored for future use.

Volume change monitoring system. The direct measurement of specimen dimensions with LVDTs can be used to find volume change. Alternatively, volume change can be monitored through the pore water volume change as measured in a burette during testing of a saturated specimen under drained condition. To measure the pore water volume change, two thin nylon tubes were inserted through the drainage ports to the frame (Fig. 1). The inside ends of these tubes were placed on the specimen's bottom and top faces, and the outer ends were connected to the bottom of a burette. The top of the burette was either open to the atmosphere or connected to a back-pressure source. In order to automate the volumetric change measurements during testing, a differential pressure transducer (DPT) was used. The DPT voltage output varies with the water level changes in the burette. A calibration chart was developed and used to convert the DPT output voltages into volume change of the specimen. The DPT

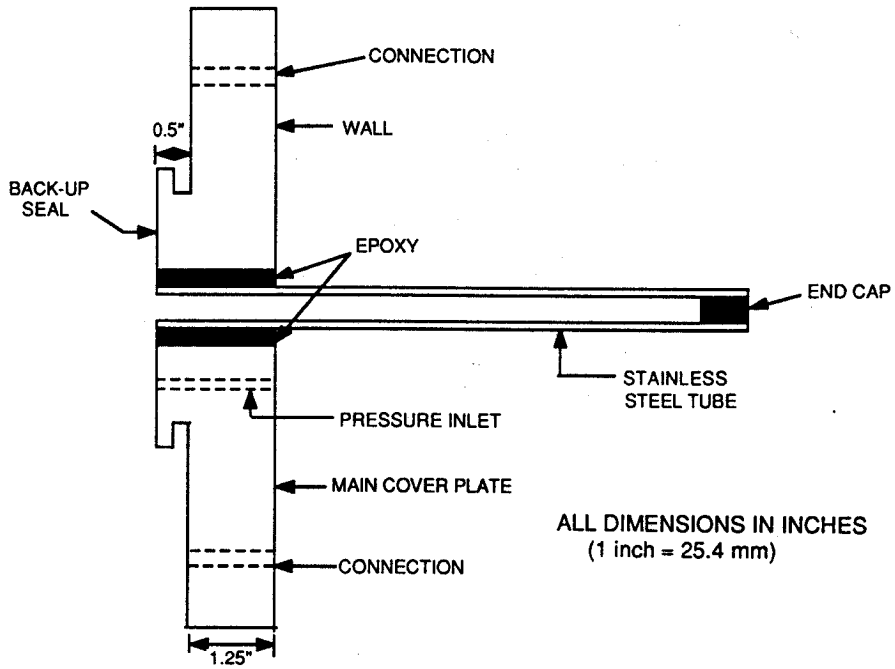

FIG. 3—*Wall assembly.*

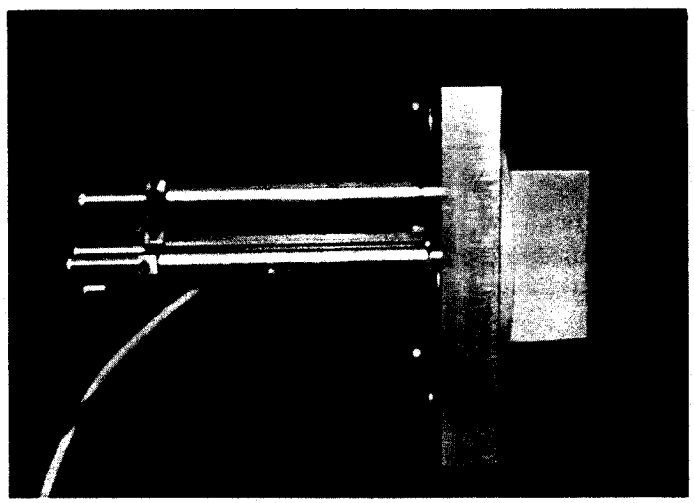

FIG. 4—*Photograph of the wall assembly.*

was connected to the data acquisition system to record its output voltage during testing.

Pore water pressure monitoring system. During undrained testing, the outer ends of the top and bottom nylon tubing passing through the ports of the frame were disconnected from the burette and conncted to a Validyne AP10 pressure transducer for pore water pressure measurement. The output voltages of the pressure transducer were recorded by the data acquisition system.

Data acquisition system. A schematic of the data acquisition system developed and used in this investigation is shown in Fig. 7. A microcomputer equipped with a direct interface card was used for data acquisition. An analog-to-digital converter, Model DM200 from Validyne comprising 19 in. (483 mm) chassis with 12-module capacity, was utilized. Three Model 517 isolated high-resolution analog input modules were used in the DM200 for analog-to-digital conversion. Each module had eight channels with input voltage ±10 V dc, 12-bit resolution, and 25μs con-

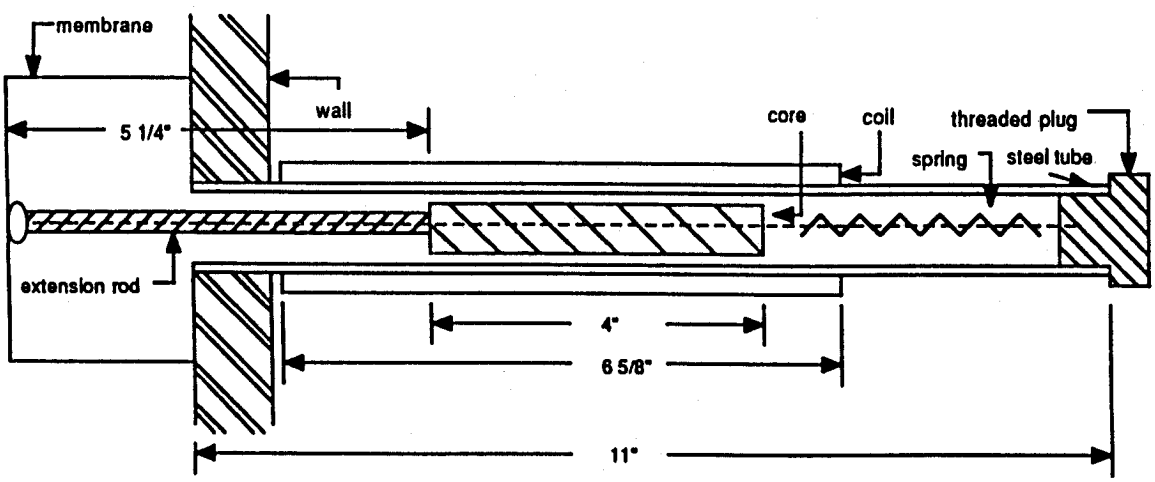

FIG. 5—*Deformation measuring system.*

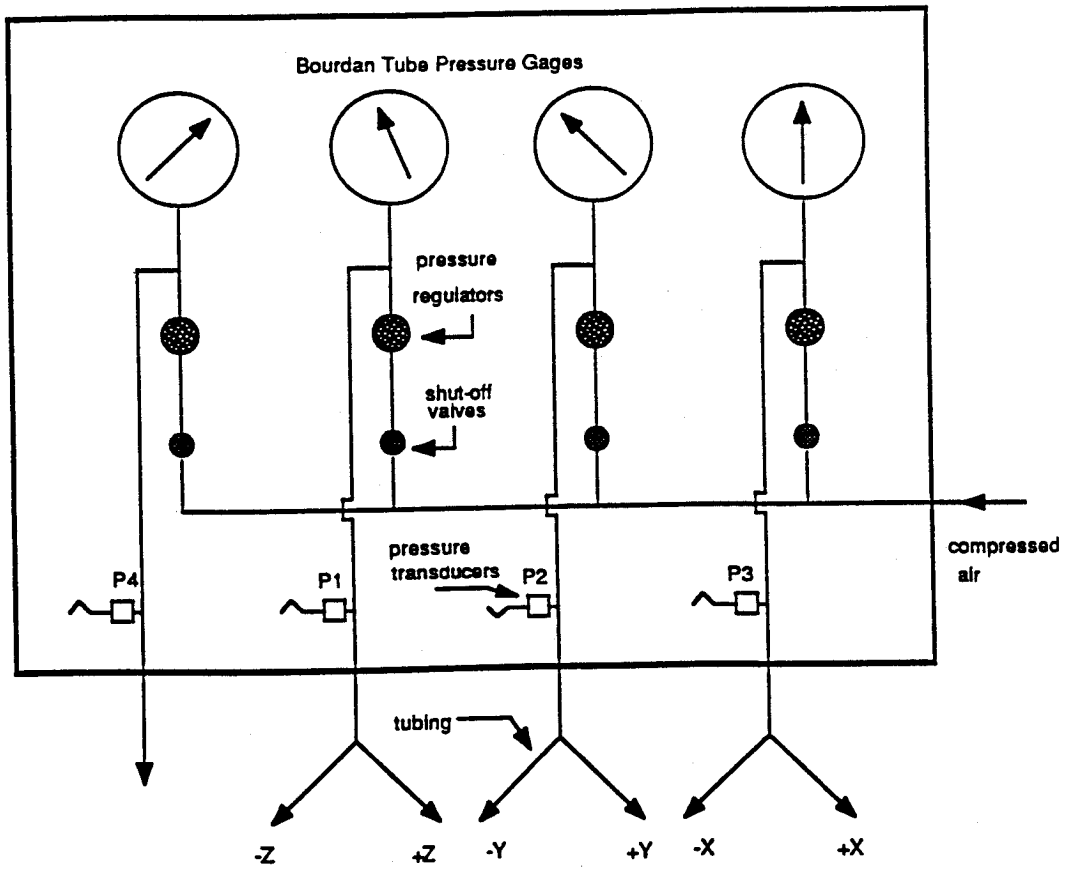

FIG. 6—*Schematic of stress application and control system.*

version time. For signal conditioning, Model MC170-32 modular (comprised of power supply and module case for 32 channels) with twelve Validyne Model CD218 dual channel carrier demodulators (each with ±10 V dc output) was used. The data acquisition system can handle the 24 LVDTs (for deformations), 3 pressure transducers (for principal stresses), 1 pressure transducer (for pore water pressure), and 1 differential pressure transducer (for volume change). A computer program was developed to calibrate the raw data (output voltages) and calculate the principal stresses, principal strains, and pore water pressure or volumetric strain.

Dynamic stress control system. The true triaxial device was also equipped with hardware for dynamic loading. A pneumatic open loop system was developed as shown schematically in Fig. 8. The system consists of a function generator, an electropneumatic transducer, volume boosters, and a series of regulators. The basic principle of the operation is to send current with a specific wave form and frequency to the electropneumatic transducer, which linearly converts the electric current to dynamic air pressure. The dynamic air pressure is amplified by a series of boosters and then applied to the specimen faces through the ports of the true triaxial wall assembly. By adjusting the d-c offset of the function generator, the desired level of static pressure can be applied before superimposing dynamic pressure on the specimen. This system can be used to apply equal cyclic pressure in one, two, or three directions on the cubical specimen.

The data acquisition system as described previously was complemented with strain gage signal conditioners (Model SG297 from Validyne) in MC170-32 and an analog-to-digital converter (Model 518 from Validyne) in DM200. The data acquisition system was used to condition and monitor the additional pressure transducers for measuring dynamic pressures. The sampling rate can be easily varied from the menu of the computer software, LABTECH-NOTEBOOK. The system can also allow the real time display of up to 16 channel responses on the computer monitor. The data can be recorded and stored simultaneously during testing.

The cyclic loading generated using the pneumatic open loop system was verified before testing a soil specimen. The output pressure was measured by a pressure transducer at various time intervals (Fig. 9). The measurements indicate that the dynamic loading system, though not very sophisticated, can generate the desired cyclic pressure with good accuracy. Very accurate response can be expected if a servocontrolled closed loop dynamic loading system is used.

Membrane effects in load transfer. The transmission of stress through the flexible membrane to the specimen was also investigated. A miniature flatline pressure transducer [EPL-125, low profile with 0.125-in. (3.175-mm) diameter and 0.04 in. (1.016 mm) thickness] was mounted to the top surface of a 4-in. (10.6-cm) wood specimen. A very small size pressure transducer was selected so that its effect on the specimen would be minimal. The wirings for the transducer were taken through the diagonal ports of the cubical frame. The wood specimen was seated in the true triaxial device and subjected to a hydrostatic pressure. A sinusoidal cyclic pressure was then superimposed in the vertical direction. Three external pressure transducers were used to measure the pressures in three directions. The outputs of the

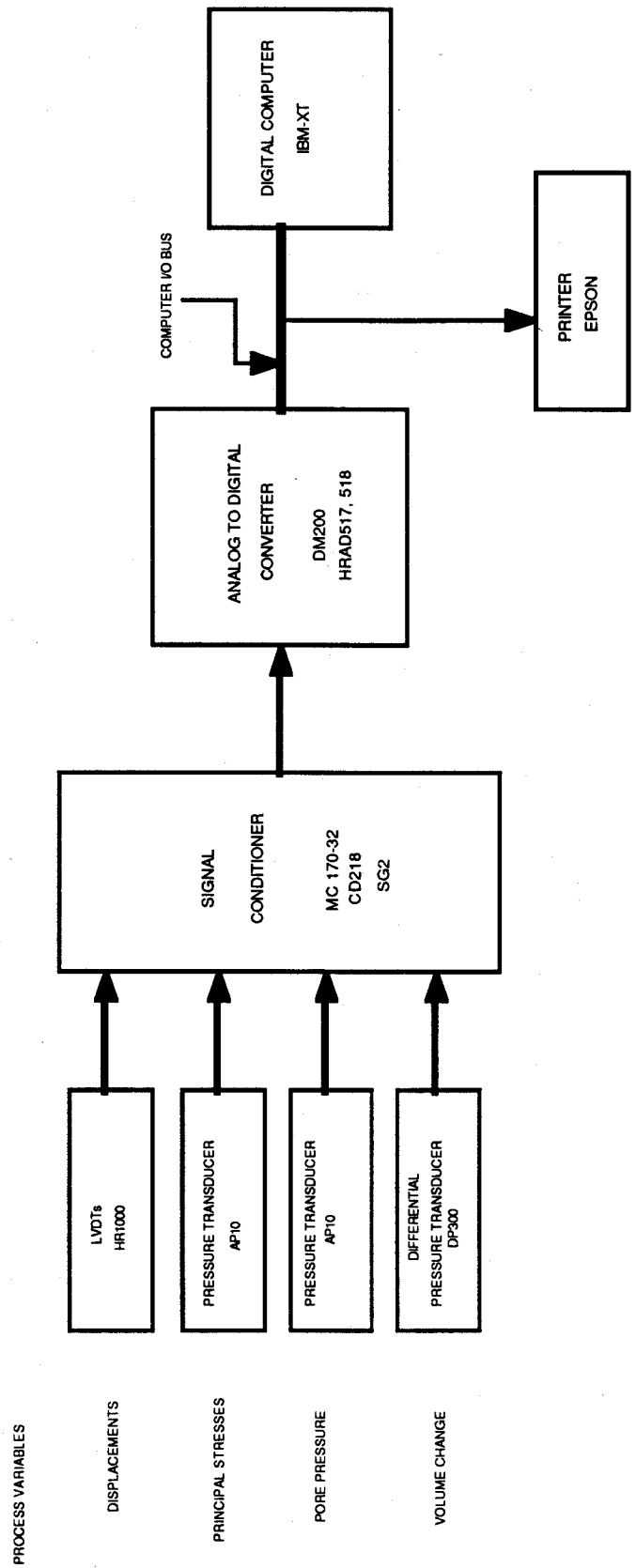

FIG. 7—*Schematic of data acquisition system.*

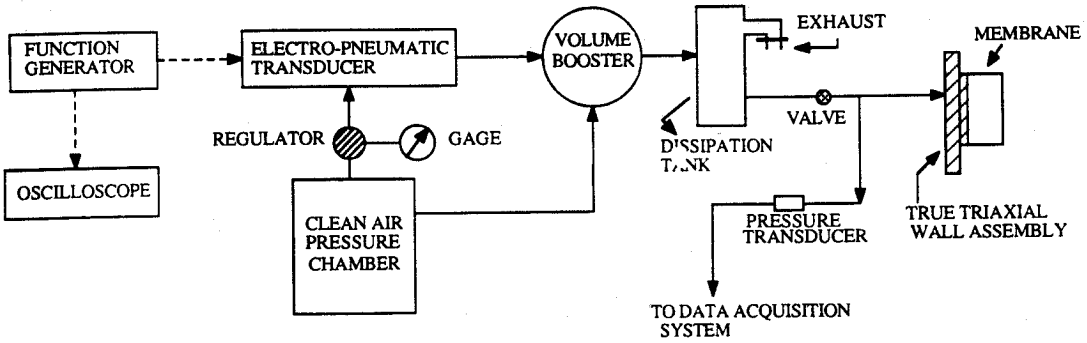

FIG. 8—*Schematic of dynamic loading system.*

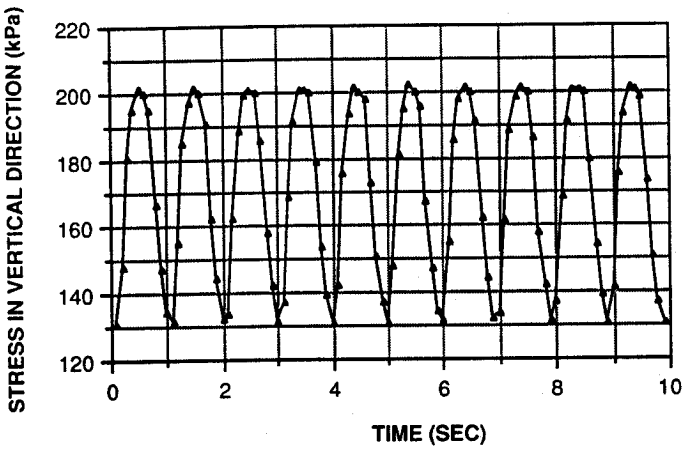

FIG. 9—*Pneumatic stress output.*

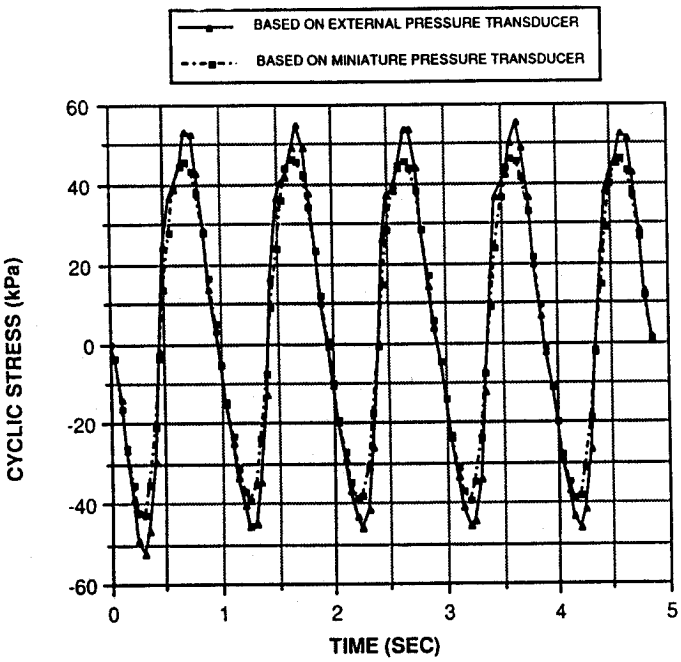

FIG. 10—*Cyclic test on a wood specimen.*

external pressure transducers and the miniature pressure transducer mounted on the specimen's surface were monitored and recorded by the data acquisition system. The measured responses of the external pressure transducer for vertical direction and the miniature transducer (sandwiched between the membrane and the specimen) were compared in Fig. 10. The results indicate that the membrane was transferring the cyclic air pressure to the specimen quite well. In addition to the wood specimen, uncemented and cemented sand specimens were also tested by placing the miniature pressure transducer on the top surface of the specimens. These results also revealed that the resistance of the membranes was negligible (Reddy 1990).

Test Program

The true triaxial device was used to investigate the constitutive behavior of cemented sand under different stress paths. The investigation was aimed at complementing the previous studies on cemented sands at Illinois Institute of Technology using conventional axisymmetric triaxial apparatus (Saxena et al. 1988a, c). The materials used in this investigation were Monterey No. 0/30 sand and Portland Cement Type I. The grain-size distribution of the sand is shown in Fig. 11. Portland cement was chosen because it was commercially available and is used widely in practice. In this study, 2% of cement content (based on dry weight of sand) was chosen because: (1) use of more than 2% cement for improving static and dynamic strength of sands has been found to be overly conservative (Saxena et al. 1988a, b, c); (2) use of more than 2% cement for artificial cementation of sands may not be economically viable for practical purposes; and (3) less than 2% cement content has been found to be insufficient to allow for effective dispersion of cement throughout the sand (Mitchell 1981). Another important variable, initial relative density, is taken equal to 43% to represent a loose to medium dense condition of sand. Higher densities were not considered because cementation for such sands may not be necessary.

Specimen Preparation and Seating Specimen in Space Frame

Four-inch (10.2-cm) cubical specimens were prepared by a method similar to that of undercompaction (Ladd 1978) inside a specially manufactured mold as shown in Fig. 12. The method of undercompaction was chosen because specimens prepared with this method were more reproducible than those made with vibration or pluviation techniques. Also, particle segregation was minimized during preparation. In this study, the specimens were prepared in six layers. The lower layers were placed in a relatively loose condition (undercompacted). As the subsequent layers were compacted, the previous layers were densified further.

The undercompaction required for each layer was calculated using the following equation (Ladd 1978)

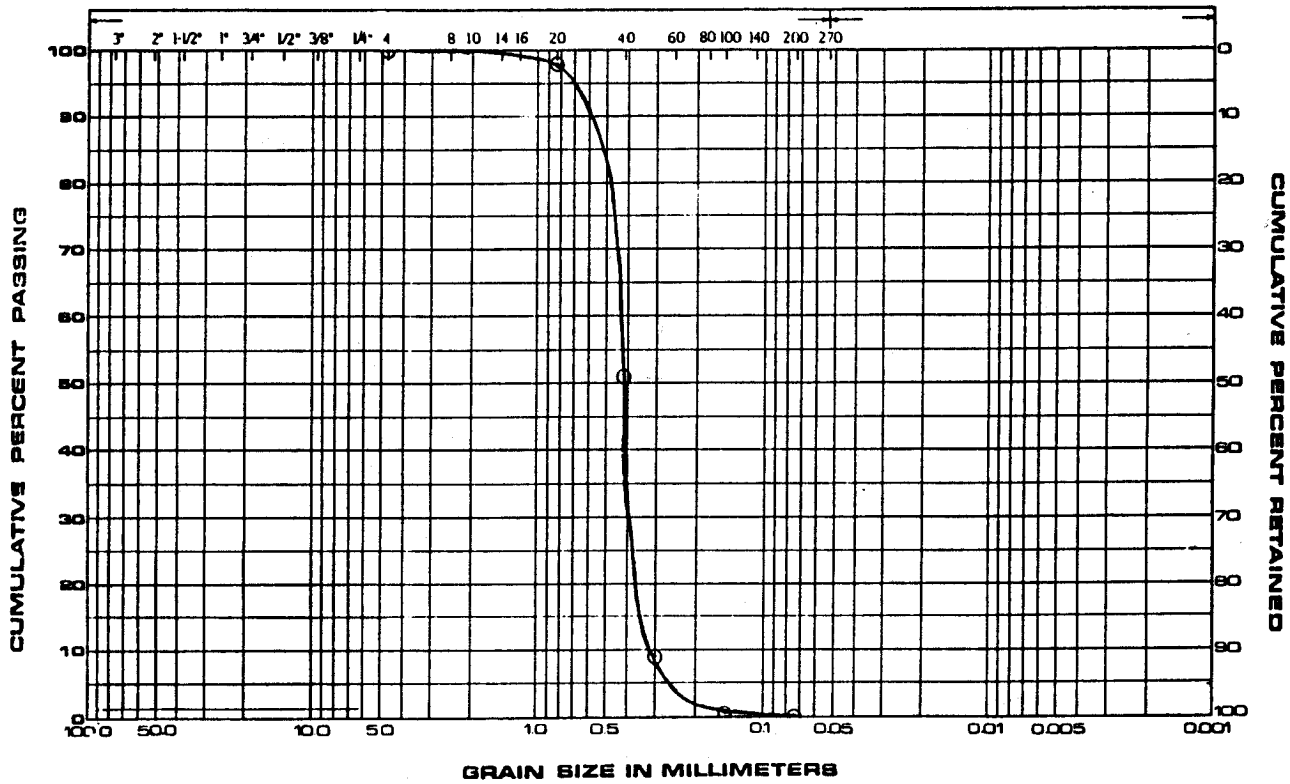

FIG. 11—*Grain-size distribution for Monterey No. 0/30 sand.*

$$U_n = U_{ni} - (U_{ni} - U_{nt}) \frac{(n - 1)}{(n_t - 1)} \quad (1)$$

where

U_n = degree of undercompaction for layer n
U_{ni} = degree of undercompaction for bottom (or first layer),
U_{nt} = degree of undercompaction for top (or final) layer,
n_t = total number of layers, and
n = layer under consideration.

In this investigation, $U_{ni} = 6\%$ and $U_{nt} = 0\%$ were chosen. Using these degrees of undercompaction, height of the specimen at the top of nth layer was computed using the following equation

$$h_n = \frac{h_t}{n_t}\left(n + \frac{U_n}{100}\right) \quad (2)$$

where h_t = total height of the specimen, and h_n = height of specimen at nth layer. During specimen preparation, 8% water by weight was added to the sand-cement mixture.

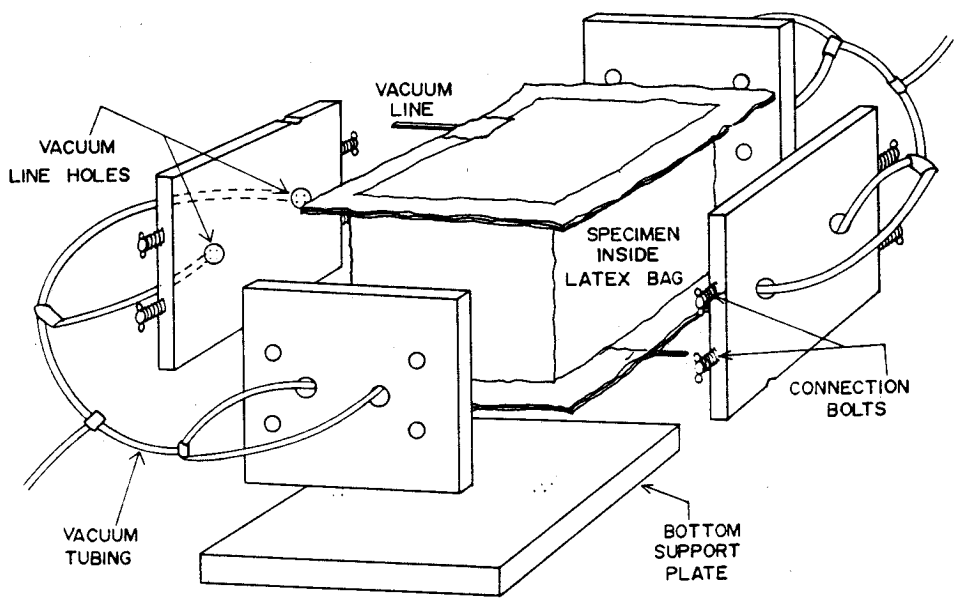

FIG. 12—*Schematic of specimen preparation mold.*

Specimen preparation and placement of specimens in the cubical frame were performed as explained below:

1. All side walls of the specimen preparation mold were assembled and outer vacuum tubes were connected (refer to Fig. 12).
2. Pieces of latex rubber membrane were glued together and then rolled onto the interior vertical sides of the mold. A thin nylon tube was inserted through the bottom groove of the mold. The inside end of the tube was covered with a filter paper. Another piece of latex rubber was placed on the bottom support plate and glued to the side pieces of latex rubber.
3. Suction was applied through the vacuum ports to hold the latex rubber tight to the sides of the mold without wrinkles.
4. Layer after layer of the sand-cement-water mixture was placed in the mold and compacted.
5. After compaction, the sample was allowed to cure for 14 days. A thin nylon tube similar to the one at the specimen's bottom was placed on top of the sample and a piece of latex rubber was placed on top of the mold and glued to the inside latex rubber to seal the sample completely. A vacuum of -7 to -14 kPa was found to be sufficient for necessary handling purposes.
6. The surfaces of the membranes (fixed to the true triaxial wall assemblies) were lubricated with a thin film of grease to eliminate friction. The specimen was then carefully placed into the cell.
7. All the wall assemblies were attached to the frame, and the LVDTs were positioned to be within their range of measurement.

Test Procedure

Saturation and consolidation of specimens were performed following methods similar to that of the conventional triaxial test. After the specimen was saturated (using back pressure) and consolidated, any desired stress path could be applied on the specimen. The specimen could be subjected to a stress path by manually controlling the three independent pressure regulators on the stress control system (Fig. 6). In this investigation, all the tests were conducted under drained condition. The applied back pressure was maintained constant during an entire test. All data during testing were recorded and stored by the data acquisition system.

It may be mentioned that no friction on the faces of the specimen was assumed; therefore, the normal stresses (σ_x, σ_y, σ_z) and strains (ε_x, ε_y, ε_z) on the sides of the specimen are principal components of the stress and strain tensors. Here, the subscripts x and y refer to the horizontal directions and z refers to the vertical direction.

The stress paths imposed on the specimens in this study included:

1. Hydrostatic compression tests (HC tests).
2. Conventional triaxial compression tests (CTC tests).
3. Shear tests on octahedral planes with various b values.

where stress ratio, b, is defined as $(\sigma_2 - \sigma_1)/(\sigma_1 - \sigma_3)$; σ_1, σ_2 and σ_3 are the major, intermediate, and minor principal stresses, respectively. These stress paths are shown graphically in Fig. 13. Hydrostatic and conventional triaxial test results are generally required to determine parameters for several constitutive models. Tests on octahedral planes were conducted by loading the specimens hydrostatically to the octahedral normal stress equal to

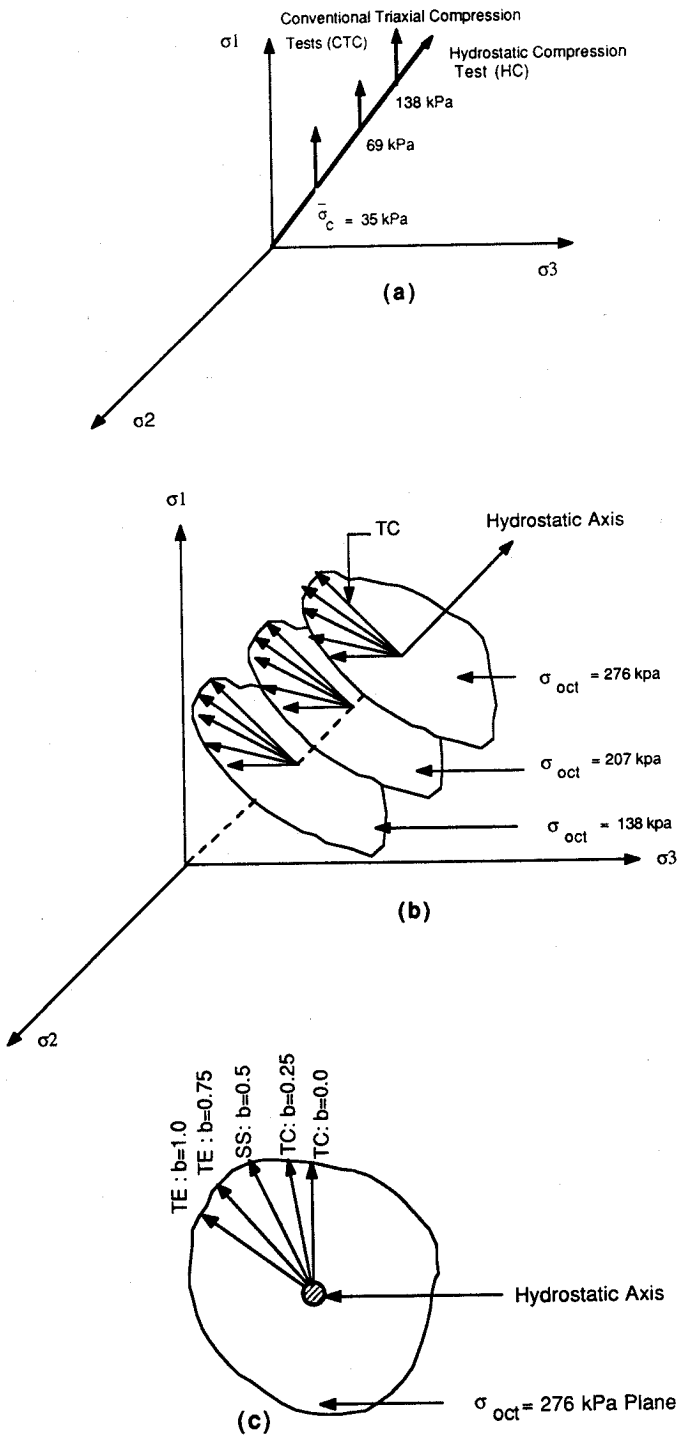

Notation:

b= (σ2 − σ3) / (σ1 - σ3)

TC = Triaxial Compression

SS= Simple Shear

TE= Triaxial Extension

FIG. 13—*Stress paths studied.*

one of three selected levels, 20, 30, or 40 psi (138, 207, or 276 kPa) and then subsequently following a monotonic shear stress path to stay on the octahedral plane along different directions defined by the value of b as shown in Fig. 13. The superposition of a pure shear stress on an initially hydrostatic state permitted the investigation of the effect of a three-dimensional shear stress state on the stress-strain behavior. Using these test results, the shape of the ultimate failure envelope could be investigated.

Test Results and Discussion

The hydrostatic compression (HC) test results are presented in Fig. 14. The three principal strains measured are plotted against mean pressure in (a), and the volumetric strain versus mean pressure is shown in (b) of the figure. Figure 15 shows the conventional triaxial compression (CTC) test results. The measured principal strains are plotted against octahedral shear stress in (a), while major principal strain versus volumetric strain is plotted in (b) of the figure. The CTC tests were performed under effective confining pressures of 5, 10, and 20 psi (35, 69, and 138 kPa). In these tests, the intermediate and minor principal stresses were maintained constant while increasing the major principal stress. It can be seen from Figure 15(a) that the principal strains in x and y directions (ε_x and ε_y) are expansive and equal when the stress in z direction is increased. The results show no significant variation of ε_x and ε_y for each of the three tests. The major principal strain (ε_z) is always compressive. The initial stress-strain response is stiffer and strains are smaller. The volumetric strains are predominantly dilative.

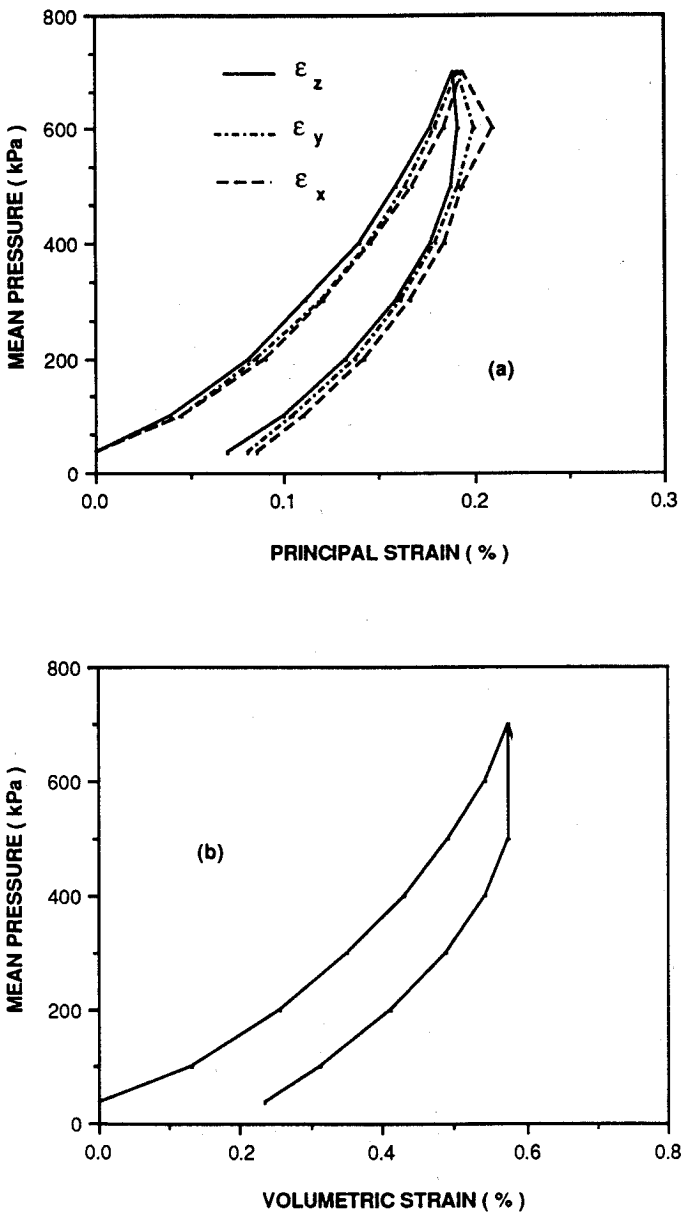

FIG. 14—*Hydrostatic compression test results.*

To investigate the response of the cemented sand under pure shear conditions, the specimens were initially loaded hydrostatically to a prescribed octahedral normal stress (σ_{oct}). Subsequently, shear stress was applied while maintaining σ_{oct} constant. Five different shear stress paths defined by b = 0.0, 0.25, 0.5, 0.75, and 1.0 were considered (refer to Fig. 13). These test results are presented and discussed in the following paragraphs.

In b = 0 tests, values of two principal stresses were equally decreased while the other stress was increased such that σ_{oct} is constant. Figure 16 shows the results from b = 0 tests performed on cemented sand specimens. As the minor and intermediate principal stresses were decreased equally, the corresponding strains (ε_x, ε_y) were found equal and expansive, indicating isotropic behavior. The major principal stress was increased during testing; consequently, its corresponding strain (ε_z) is compressive. The volumetric response is generally dilative. It can be seen also that the dilation in tests with σ_{oct} = 20 psi (138 kPa) is less as compared to CTC tests with σ_c = 20 psi (138 kPa).

Figure 17 shows b = 0.25 test results on cemented sand. These tests were conducted with σ_{oct} = 30 and 40 psi (207 and 276 kPa). From Figure 17(a), it can be seen that the three principal strains are different because the three principal stresses were different during testing. The major principal strain (ε_z) is compressive, while the minor principal stress (ε_x) is expansive. The intermediate principal strain (ε_y) is very small during the initial loading process and is expansive at higher stress levels. From part (b) of the figure, the volumetric strains are generally dilative. The dilatancy of the cemented sand in these tests is less as compared to the b = 0 tests.

In b = 0.5 tests, the major principal stress (σ_z) was increased and at the same time the minor principal stress (σ_x) was decreased. The intermediate principal stress (σ_y) was maintained constant. These tests were performed with σ_{oct} = 20, 30, and 40 psi (138, 207, and 276 kPa), and the results obtained are shown in Fig. 18. The major principal strain is (ε_z) compressive, the minor principal strain (ε_x) is expansive, and the intermediate principal strain (ε_y) is almost zero. As the intermediate principal strain is very small, this type of test condition closely corresponds to a plane strain condition. The dilative volumetric strains in these tests are higher than in b = 0 and b = 0.25 tests.

The test results for the cemented sand based on b = 0.75 tests are shown in Fig. 19. Results show contraction in the direction of major principal stress and expansion in the direction of minor principal stress. The intermediate principal strain is slightly compressive in these tests.

In b = 1 tests, the intermediate and major principal stresses (σ_y, σ_z) were equal and increased equally while the minor principal stress (σ_x) was decreased. Figure 20 presents the b = 1.0 test results for cemented sand. The compressive strains, ε_y and ε_z, are nearly equal because of σ_y = σ_z. The minor principal

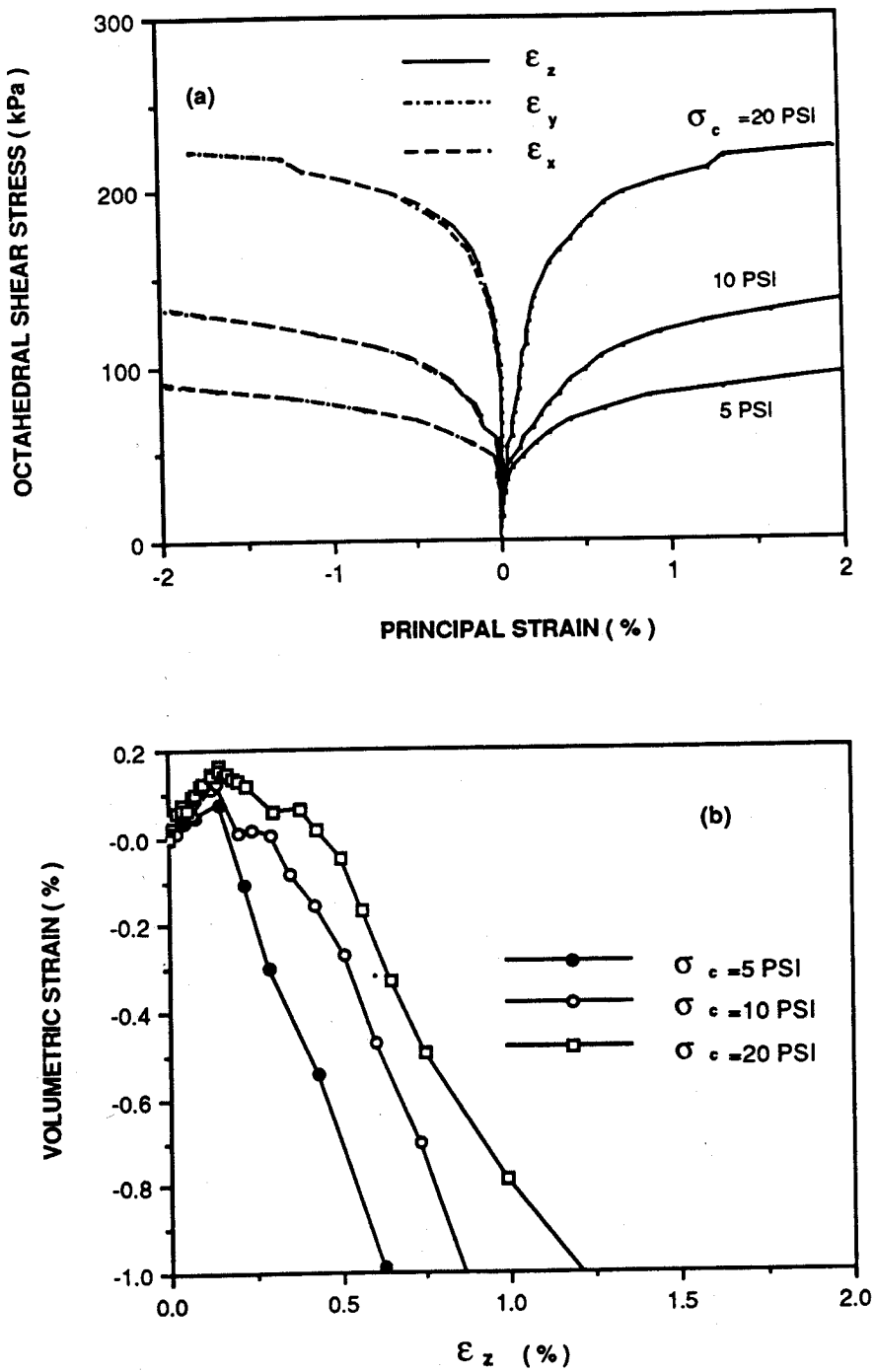

FIG. 15—*Conventional triaxial compression test results.*

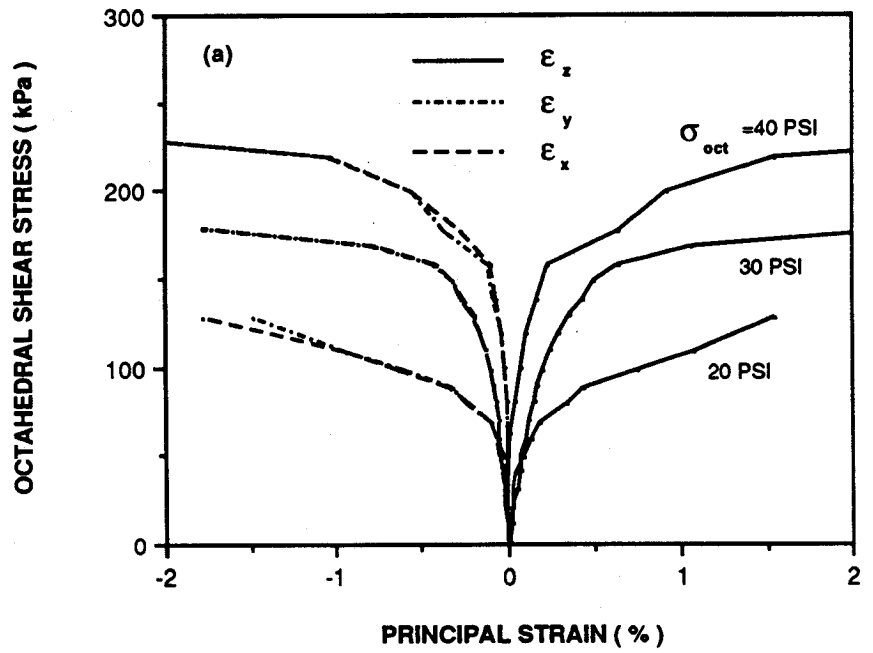

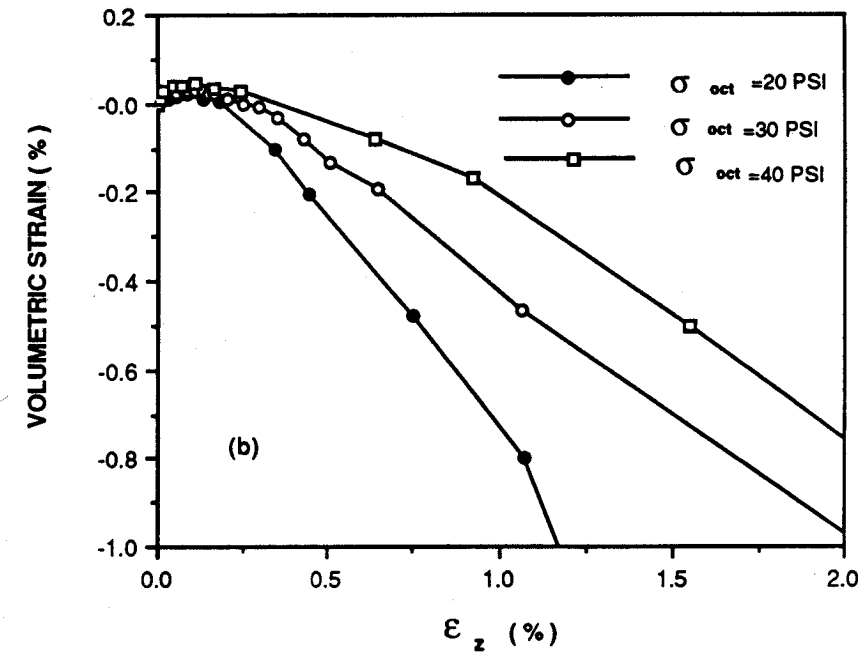

FIG. 16—b = *0 test results.*

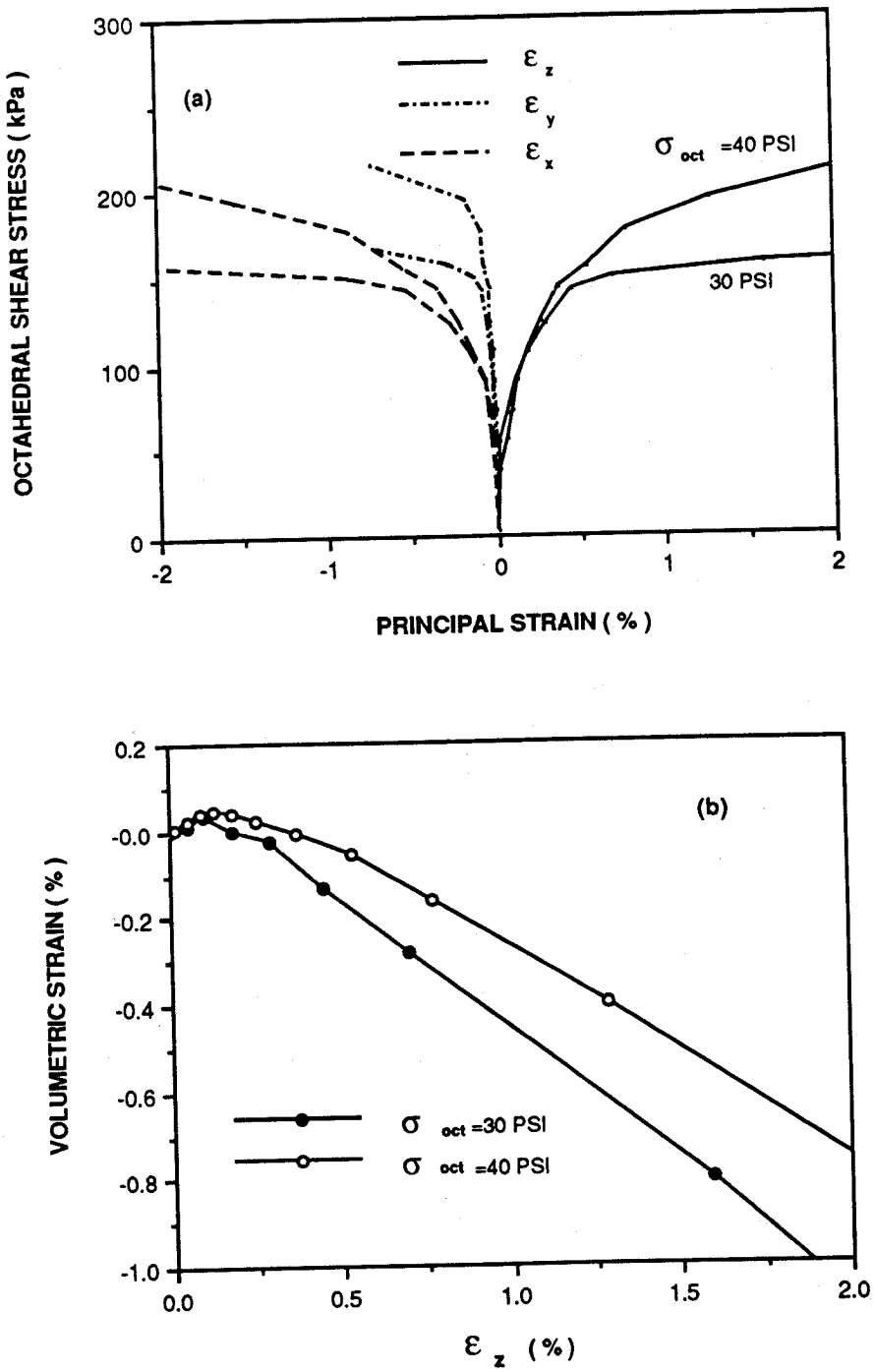

FIG. 17—b = *0.25 test results.*

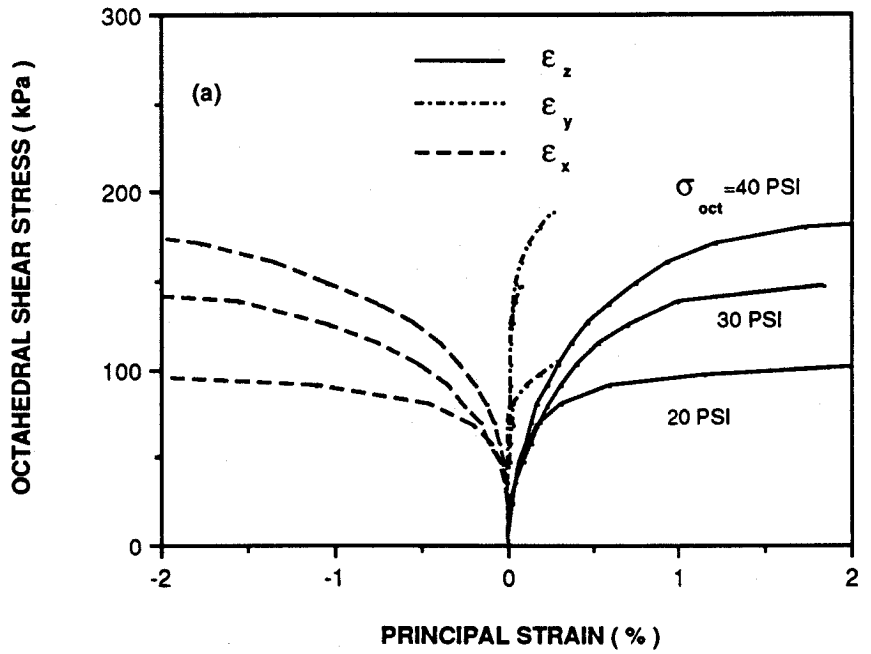

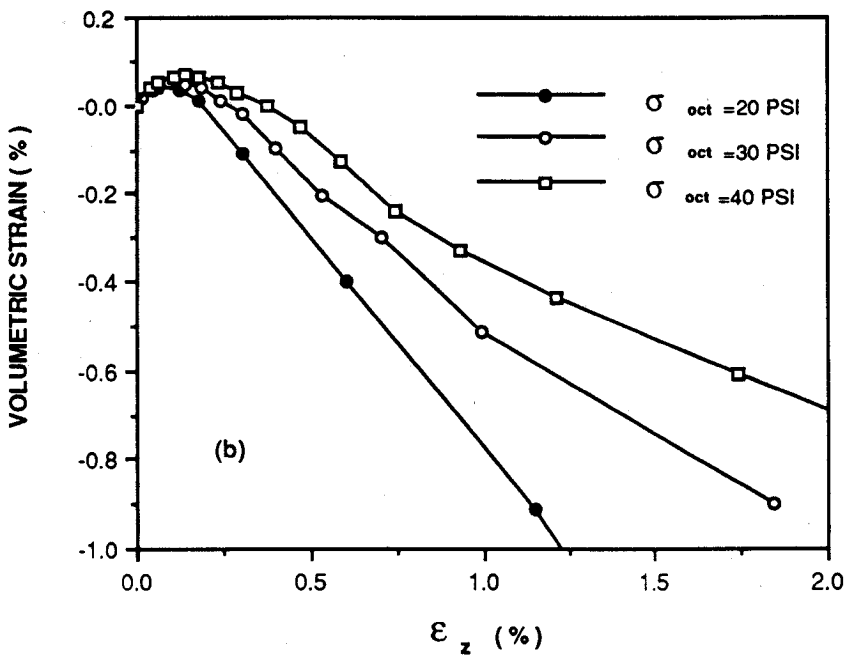

FIG. 18—b = *0.5 test results.*

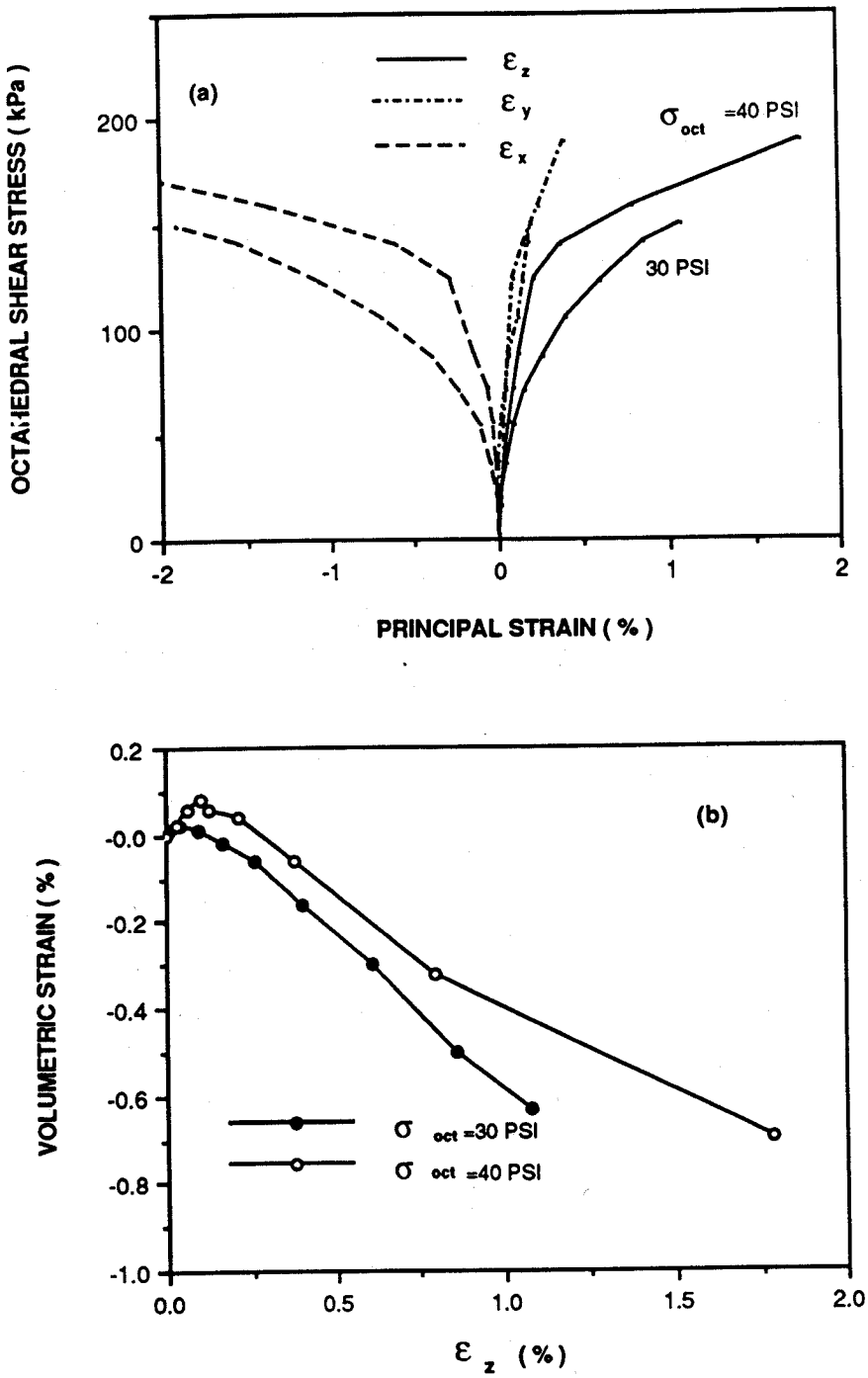

FIG. 19—b = *0.75 test results.*

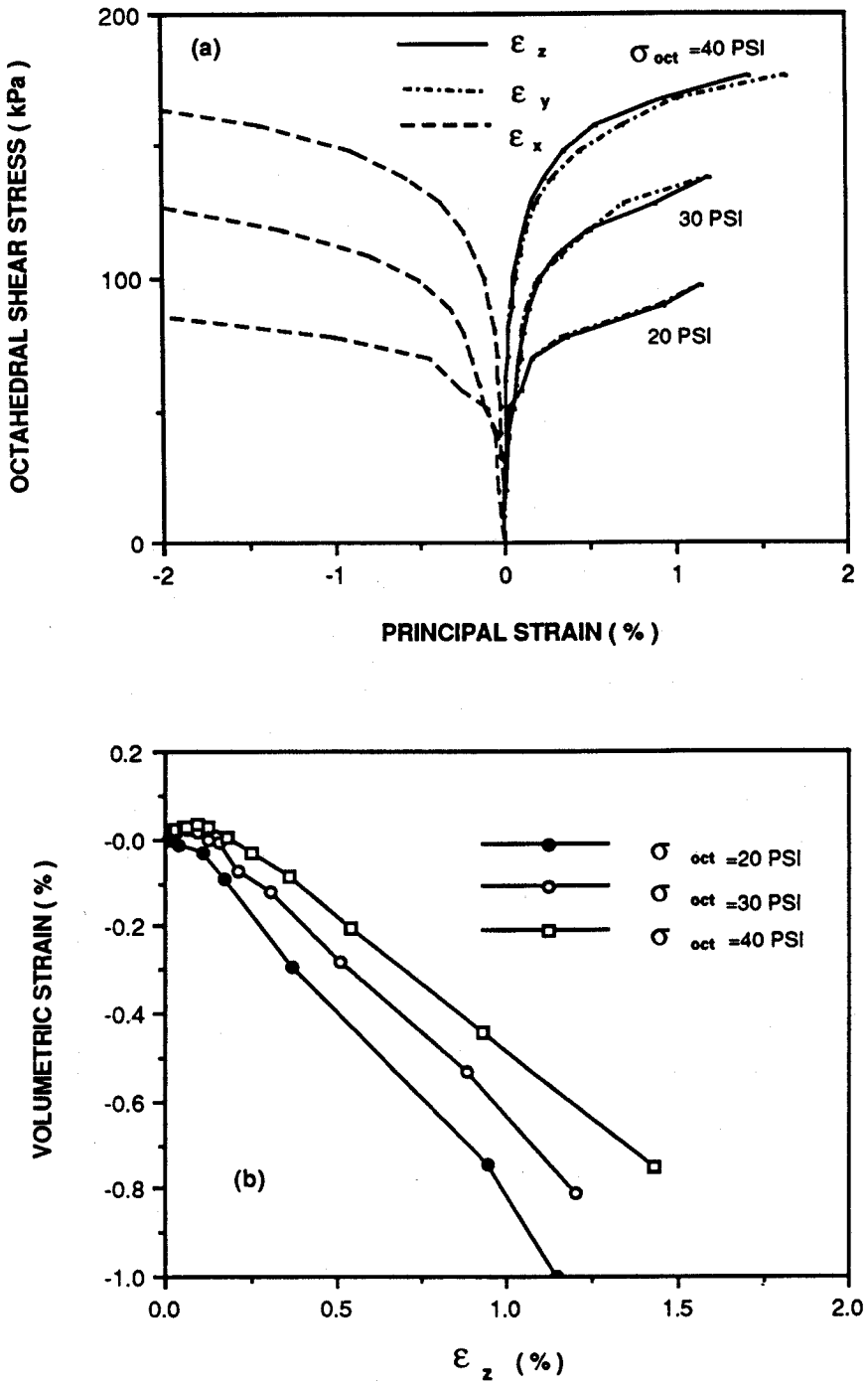

FIG. 20—b = *1.0 test results.*

strain, ε_x is expansive. The volumetric strains in these tests are also predominantly dilative.

Failure Envelope

The results from conventional triaxial, triaxial compression, and triaxial extension tests are plotted on a triaxial plane as shown in Fig. 21(*a*). The shape of the failure surface for cemented sand is similar to that reported for uncemented sand (Lade and Duncan 1973) except that it starts on the negative side, reflecting slight tensile strength. The projection of failure surface, based on tests along different shear stress paths, on the octahedral plane (or π plane) is shown in Fig. 21(*b*). The failure surfaces on the triaxial and octahedral planes show that the failure envelope for cemented sand is cone shaped. The coordinate of the envelope from hydrostatic depends on the *b* value, which shows the stress path dependency.

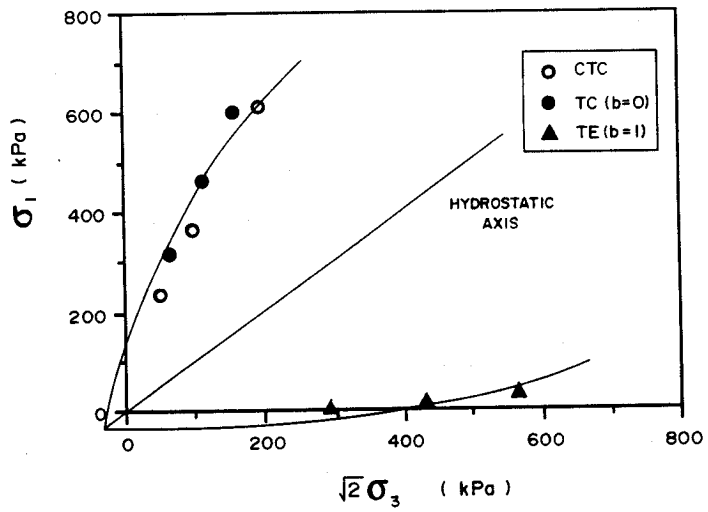

FIG. 21(*a*)—*Failure surface on the triaxial plane.*

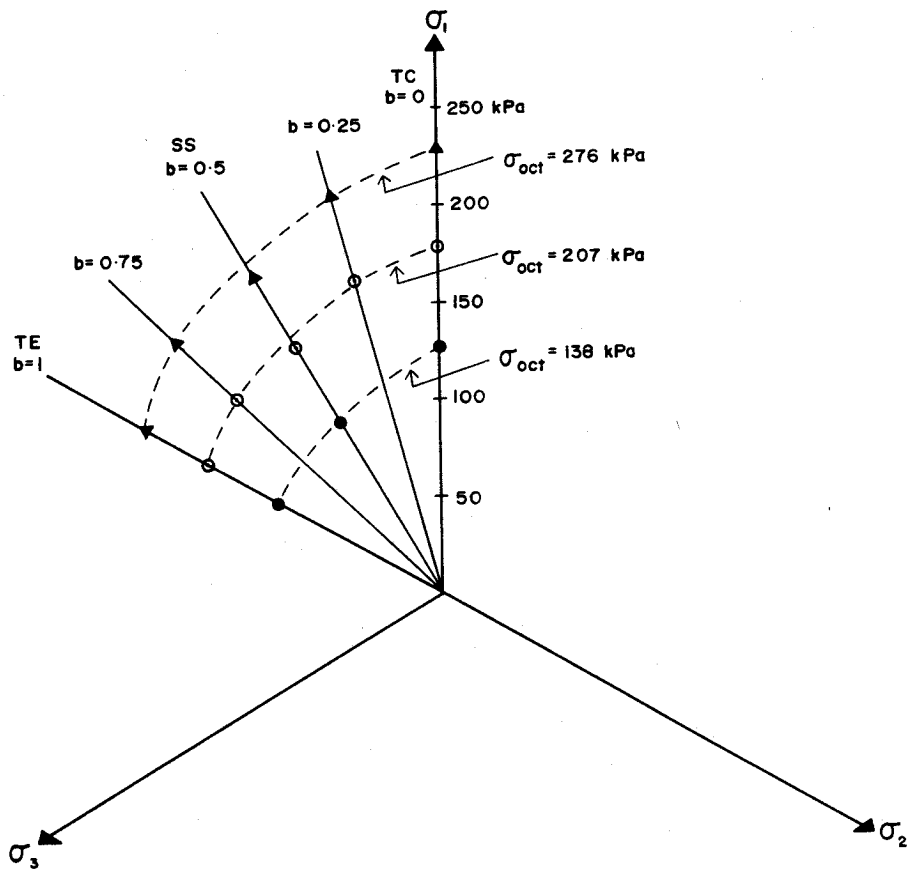

FIG. 21(*b*)—*Failure surface on the octahedral plane.*

Summary and Conclusions

A stress-controlled, flexible boundary, true triaxial apparatus was developed to investigate the behavior of cemented sand under various stress paths which are not achievable using conventional axisymmetric triaxial apparatus. The stress paths included hydrostatic compression, conventional triaxial compression, and tests along different directions on different octahedral planes. The test results indicate that: (1) cemented sand contracts in the direction of major principal stress, expands in the direction of minor principal stress, and changes from expansive to compressive in the direction of the intermediate principal stress as b changes from 0 to 1; (2) cemented sand exhibits predominantly dilatant response—the dilation increases as the b value changes from 0 to 1; and (3) the shape of failure envelope for cemented sand is similar to the one for uncemented sand on triaxial and octahedral planes. The failure envelope on triaxial plane reflects the tensile strength of cemented sand. On the octahedral plane, the failure envelope is cone shaped with a triangular (with curved corners) cross section.

Acknowledgments

The first author wishes to express his appreciation and gratitude to the late Professor Saxena (the second author) for providing advice, encouragement, and financial support during this study.

References

Airey, D. W., and Wood, D. M., 1988, "The Cambridge True Triaxial Apparatus," *Advanced Triaxial Testing of Soil and Rock, STP 977*, ASTM, Philadelphia, pp. 796–805.

Arthur, J. R. F., 1988, "Cubical Devices: Versatility and Constraints," *Advanced Triaxial Testing of Soil and Rock, STP 977*, ASTM, Philadelphia, pp. 743–765.

Green, G. E., 1971, "Strength and Deformation of Sand Measured in an Independent Stress Control Cell," *Stress-Strain Behavior of Soils*, Proceedings of the Roscoe Memorial Symposium, G. T. Foulis & Co. Ltd., Cambridge, England, pp. 285–323.

Hambley, E. C., 1969, "A New Triaxial Apparatus," *Geotechnique*, Vol. 19, No. 2, pp. 307–309.

Ko, H.-Y., and Scott, R. F., 1967, "A New Soil Testing Apparatus," *Geotechnique*, Vol. 17, No. 1, pp. 40–57.

Ladd, R. S., 1978, "Preparing Test Specimens Using Undercompaction," *Geotechnical Testing Journal*, Vol. 1, No. 1, pp. 16–23.

Lade, P. V., and Duncan, J. M., 1973, "Cubical Triaxial Tests on Cohesionless Soil," *Journal of the Soil Mechanic Foundation Division, ASCE*, Vol. 99, SM10, pp. 793–812.

Mitchell, J. K., April 1981, "Soil Improvement Methods and Their Application in Civil Engineering," Sixteenth Henry M. Shaw Lecture, North Carolina State University, Raleigh, NC.

Reddy, K. R., May 1990, "Behavior of Cemented Sands Under Three-Dimensional Loadings," Ph.D. thesis, Department of Civil Engineering, Illinois Institute of Technology, Chicago, IL.

Saxena, S. K., Reddy, K. R., and Avramidis, A., 1988a, "Static Behavior of Artificially Cemented Sand," *Indian Geotechnical Journal*, Vol. 18, No. 2, pp. 111–141.

Saxena, S. K., Avramidis, A., and Reddy, K. R., 1988b, "Dynamic Moduli and Damping Ratios for Cemented Sands at Low Strains," *Canadian Geotechnical Journal*, Vol. 25, No. 2, pp. 353–368.

Saxena, S. K., Reddy, K. R., and Avramidis, A., 1988c, "Liquefaction Resistance of Artificially Cemented Sand," *Journal of Geotechnical Engineering, ASCE*, Vol. 114, No. GT12, pp. 1395–1413.

Sture, S., and Desai, C. S., 1979, "Fluid Cushion Truly Triaxial or Multiaxial Testing Device," *Geotechnical Testing Journal*, Vol. 2, No. 1, pp. 20–33.

Sture, S., May 1979, "Development of Multiaxial Cubical Test Device with Pore Water Pressure Monitoring Facilities," Report No. VPI-E-79.18, Department of Civil Engineering, Virginia Polytechnic Institute and State University, Blacksburg, VA.